Plasma sheet access to geosynchronous orbit: Generalization to numerical global field models

H. Korth and M. F. Thomsen

Los Alamos National Laboratory, Los Alamos, New Mexico

Abstract. A previous statistical analysis of the geosynchronous particle environment by *Korth et al.* [1999] showed that the particle fluxes are well organized by local time and the geomagnetic activity as measured by the *Kp* index. Regions of high and low fluxes at geosynchronous orbit are separated from each other by distinct boundaries, approximately matching the Alfvén boundary crossings of the geosynchronous satellites calculated analytically from a Volland-Stern electric potential and a dipole magnetic field. Expanding the analysis technique from the previous work to arbitrary, numerical electric and magnetic field models, we reevaluate the Alfvén boundary crossings using several available global electric potential models and considering external magnetic field contributions. The more sophisticated numerical models do not do a better job of explaining the observed average access of plasma sheet material to the geosynchronous region than does the simple analytical model.

1. Introduction

Particle motion in the inner magnetosphere of the Earth has been well studied for several decades, and particle drift patterns are principally determined by the electric and magnetic field distributions. As discussed by many authors, two classes of drift trajectories form from these contributions [e.g., *Roederer*, 1970]. Near the Earth where the corotation field dominates there is a class of closed drift trajectories. At larger distances from the Earth, drift trajectories are open, and fresh plasma sheet material may be transported from the geomagnetic tail toward and around the Earth. Thus, at a given location in the inner magnetosphere, high particle fluxes in the plasma sheet energy range are associated with open drift trajectories, while low fluxes are associated with closed trajectories. The open and closed regions are separated from each other by the Alfvén layer [e.g., *Schield et al.*, 1969, and references therein]. A statistical survey of the geosynchronous particle fluxes shows distinct boundaries, the location of which depends on the particle species and magnetic moment, as well as the geomagnetic activity level and local time [*Korth et al.*, 1999]. The statistical boundaries can be interpreted as Alfvén layer locations at geosynchronous orbit separating open and closed regions. Thus they ultimately give valuable information about the delivery of plasma sheet material from the magnetotail to the near-Earth region in a statistical sense, an important aspect in predicting space weather. Previous work by *Korth et al.* [1999] (hereinafter called paper 1) compared the observed flux boundaries to geosynchronous Alfvén layer crossings, as predicted by a Volland-Stern electric potential [*Volland*, 1973, 1975, 1978; *Stern*, 1975] and a dipole magnetic field. Even though time variability of the geomagnetic activity is believed to play a considerable role in the transport process, the study showed a surprisingly good match between observed and theoretical boundaries. The Volland-Stern and dipole models are very simple. Nowadays, much more sophisticated models exist, and the question arises of whether these models can improve the drift picture in the inner magnetosphere and do even better at reproducing the statistical boundaries. This issue will be addressed in the present paper.

2. Models

2.1. Alfvén Layer Model

The Volland-Stern and dipole model used in paper 1 are given in the form of analytical expressions, leading to a likewise analytical description of the Alfvén boundaries. Here we generalize to nonanalytical, semiempirical models, which requires a modified approach for obtaining the theoretical boundaries. Using the (U, B, K) formalism, the boundary locations can be easily obtained, as shown in pa-

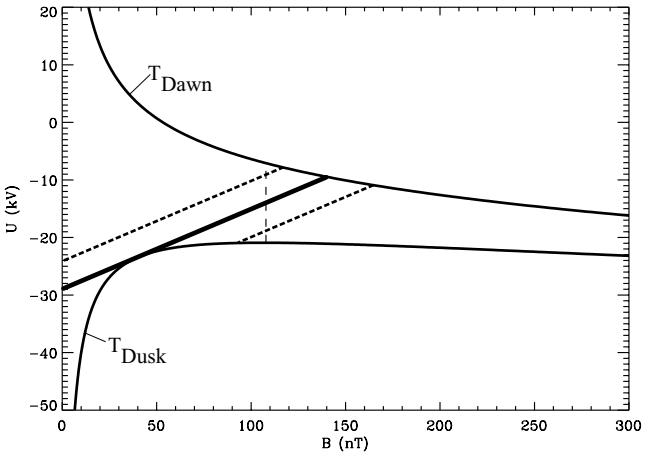

Figure 1. Example scenario for the (U, B) coordinate system. The separators, labeled $T_{\rm Dawn}$ and $T_{\rm Dusk}$, are calculated for the Volland-Stern and dipole model combination using a shielding factor of $\gamma = 2$ and a geomagnetic activity level of $Kp = 3$. Geosynchronous orbit is shown as a dashed vertical line at a magnetic field magnitude of ~ 100 nT. The dotted lines show examples for open and closed drift trajectories of 15-keV electrons. Particle trajectories extending to low magnetic field values near the U axis have their origin in the far magnetotail and can be considered open. Drift trajectories connected to the terminators at both ends perform cyclic orbits between the separators and are thus closed. The Alfvén layer separating the two regions is shown as a thick solid line.

per 1 and references therein. Describing particle locations in terms of the electric potential U, the magnitude of the magnetic field at the mirror point B, and the modified second adiabatic invariant K leads to drift trajectories and Alfvén layers that can be represented by straight lines. Assuming equatorially mirroring particles ($K = 0$), the K coordinate may be omitted, and all particle locations can be described by (U, B) coordinate pairs. The space of valid combinations of U and B is limited by two separators, also called terminators in this paper (see Figure 1). The Cartesian locus of the separators is given by the extrema of the magnetic field on the equipotentials of the electric field as illustrated by Figure 2. Figure 2 shows a two-dimensional projection of the $\vec{B} \cdot \nabla B = 0$ surface, also referred to as the "bounce center surface" [cf. *Vogt and Glaßmeier*, 2000], with schematic isocontours of B represented by dashed circles and a selected equipotential of the electric field drawn as a solid line. For a dipole magnetic field the bounce center surface coincides with the equatorial plane. A coordinate system is defined locally along the path of the electric equipotential contour with s pointing in the direction $dU = 0$ and a ρ direction perpendicular to s. In this coordinate system the gradient of the electric potential of U can be written as

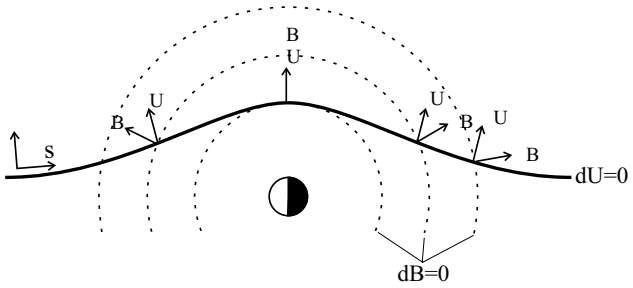

Figure 2. Relationship between gradients and isocontours in the bounce center surface. The dashed lines are isocontours of a dipolar magnetic field while the solid line represents an equipotential of the electric field. The terminators consist of loci where the magnetic field reaches an extremum on the isocontour of the electric potential. For these points the gradients of U and B are parallel.

$$\nabla U = \frac{\partial U}{\partial s}\hat{s} + \frac{\partial U}{\partial \rho}\hat{\rho}, \tag{1}$$

where $\partial U/\partial s = 0$ per definition. The gradient of the magnetic field along the contour of constant U can also be expressed in this coordinate system:

$$\nabla B = \frac{\partial B}{\partial s}\hat{s} + \frac{\partial B}{\partial \rho}\hat{\rho}. \tag{2}$$

The term $\partial B/\partial s$ in (2) becomes zero when the magnetic field reaches an extremum on the electric equipotential, causing ∇B to point solely in the ρ direction. Since the gradients of U and B, which are oriented perpendicular to their respective isocontours, are parallel in this case, the U and B isocontours must be parallel as well. Thus the contours of constant U and B are tangent at the location of an extremum which can be written as

$$(\nabla U \times \nabla B) \cdot \hat{e}_{\rm z} = 0, \tag{3}$$

where $\hat{e}_{\rm z}$ is the unit vector perpendicular to the bounce center surface. The equation used in this paper to evaluate numerically the terminator location for arbitrary models for the electric potential and the magnetic field is given through (3) as

$$\frac{\partial U}{\partial r}\frac{\partial B}{\partial \varphi} - \frac{\partial U}{\partial \varphi}\frac{\partial B}{\partial r} = 0, \tag{4}$$

where r and φ are geocentric distance and magnetic local time, respectively. Equation (4) is applied to two-dimensional grids of U and B with an extension of $20\ R_E$ from the Earth's center and a step size of $0.1\ R_E$. The magnitude of the magnetic field assigned to each grid point is the

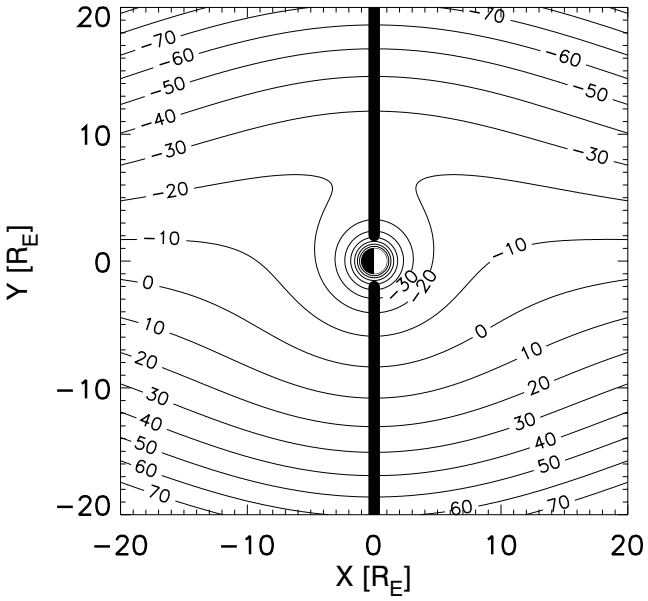

Figure 3. The separator calculated from a Volland-Stern electric potential and a dipole magnetic field in the bounce center surface is given by the dawn-dusk meridian, represented by a thick solid line. The electric potential contours, depicted by thin solid lines, are computed for a shielding factor of $\gamma = 2$ and $Kp = 3$. The potential values are given in Kilovolts. The circular isocontours of the magnetic field are omitted.

minimum value on the field line containing the grid location. The corresponding electric potentials are also obtained through a field line mapping process to the surface (i.e., the ionosphere), where the potential structure is defined for a number of the convection models we will consider. In this mapping, the field lines are assumed to be equipotentials of the electric field.

For a dipole magnetic field the bounce center surface coincides with the analysis plane. Furthermore, the Volland-Stern electric potential is directly defined for the grid, making the mapping process unnecessary. Because of the symmetry of U and B, the separator is simply given by the dawn-dusk meridian as shown in Figure 3. The field models by *McIlwain* [1986] described in section 2.2 are also defined in the equatorial plane. In this case the terminators are more complicated because of the models' asymmetry.

Using (4), the terminators for arbitrary models can be determined numerically. The Alfvén boundary can be interpreted as the last open drift trajectory, and, in principle, it is given by the straight-line trajectory that is tangent to the terminator curves (see Figure 1). However, numerical problems make this approach less successful for generalized electric and magnetic fields. Instead, for the present study, drifts are followed from numerous locations on geosynchronous orbit to see whether a location lies in the open or closed region. In this process each drift trajectory is traced in direction of decreasing B to the low magnetic field region. If a particle can escape to a threshold magnetic field of 10 nT without crossing a terminator, it is reasonable to assume the location to be in the open region. If, on the other hand, a separator crossing exists, the corresponding location at geosynchronous orbit is located in the closed region. A numerical root finder is used to detect the crossings.

2.2. Field Models

The statistical flux observations in paper 1 are organized by local time and *Kp*. In order to be able to test the field models, dependence on equal parameters is required. For some of the models, drivers other than *Kp* are used to vary the model. Thus we need to seek relationships between those parameters and *Kp*, so that *Kp* may be used as a proxy.

The magnetic field at geosynchronous orbit is dominated by the Earth's internal magnetic field. Hence the Alfvén layer calculations depend mainly on the choice for the internal field model rather than external contributions. Unless otherwise stated, we chose a tilted dipole to represent the Earth's internal field component and the Tsyganenko 89c model for the field contributions from the ring current, the magnetotail current system, and the magnetopause currents [*Tsyganenko*, 1989]. Higher-order contributions of the Earth's internal field did not lead to significant differences in the boundary locations and are therefore ignored. The Tsyganenko 89c external magnetic field model is controlled by *Kp* and the Earth's tilt angle.

A variety of electric potential models have been developed in the past. In this study, selected models by *McIlwain* [1986], *Heppner and Maynard* [1987], *Sojka et al.* [1986], and *Weimer* [1995, 1996] are considered for comparison to results acquired from the analytical Volland-Stern model. The selection criterion for the models was primarily availability. Some of the models were originally developed to describe high-latitude ionospheric convection and may not accurately describe convection at lower latitudes corresponding to the near-Earth (i.e., geosynchronous) equatorial magnetosphere. Furthermore, the entire plasma sheet maps to a very narrow latitudinal band in the ionosphere [e.g., *Pulkkinen et al.*, 1992]. Hence only small parts of the ionospheric potential models are used in our study. Nevertheless, these models are often used for studies involving particle transport in the inner magnetosphere by various authors [e.g., *Ober et al.*, 1997; *Toivanen*, 1997; *Whipple et al.*, 1998; *Quinn et al.*, 1999; Hilmer and Ginet, 2000; *Kistler and Larson*, 2000], and an exploration of their utility in this region is

warranted.

With the exception of the McIlwain E5D model, all the above mentioned (semi)empirical models provide the potential pattern in the ionosphere, requiring field line mapping to identify U on the grid. These models only consider the electric potential due to the convection electric field. The corotational contribution is not included and needs to be calculated separately. This is done by integrating the electric field induced by plasma corotating in an aligned magnetic dipole from the pole to the appropriate latitude. More accurate potential values could be obtained by taking the dipole tilt into consideration. In this study we neglect the inductive electric fields associated with the rocking of the dipole.

The global electric field model E5D was derived by McIlwain from drift-time dispersion of impulsively injected energetic particles measured by the ATS 5 satellite at geosynchronous orbit. The E5D model is more sophisticated than the one developed by Volland and Stern, yet it is still analytical. It is also the only model considered in this work that provides the electric potential in the equatorial plane. The model will be used in combination with the M2 magnetic field model [*McIlwain*, 1972], which describes the magnetic field in the neutral sheet in reasonably good agreement with quiet time geosynchronous observations [*Cummings et al.*, 1971].

The Heppner-Maynard-Rich model was developed from empirical patterns of the ionospheric convection electric field, hand-drawn by *Heppner and Maynard* [1987], which were subsequently digitized and fitted to spherical harmonics by Rich [*Rich and Maynard*, 1989]. Under southward interplanetary magnetic field (IMF) conditions a *Kp* parameterization for the model is given for three distinct states of the IMF $B_{\rm y}$ component, designated A, BC, and DE [*Heppner and Maynard*, 1987; *Rich and Maynard*, 1989]. Results shown in this paper refer to mode A, but modes BC and DE provide similar results.

The ionospheric electric potential model of Sojka is a mathematical model that also includes previously found empirical observations. The input variables are *Kp* and the IMF components $B_{\rm y}$ and $B_{\rm z}$. According to the authors of the model, the electric field has been found to correlate significantly with $B_{\rm y}$ only in the polar cap. Fortunately, the electric potential in this region is irrelevant for our application, because the field lines mapping from this part of the ionosphere are open and do not participate in the convection in the near-Earth equatorial region. The $B_{\rm z}$ component of the interplanetary magnetic field only influences the model under northward IMF conditions. Since the geomagnetic activity level is driven by the strength of the southward IMF, $B_{\rm z}$ only influences the Sojka electric convection patterns during geomagnetically quiet intervals which are concentrated at the lower end of the *Kp* scale. Thus, for our analysis the overall model dependencies can be reduced to the geomagnetic activity level expressed by the *Kp* index.

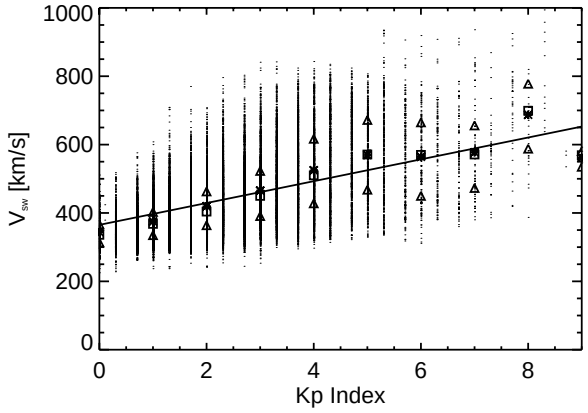

Figure 4. Relationship between hourly averaged solar wind flow speed, taken from the National Space Science Data Center (NSSDC) OMNIWeb database, and *Kp*. Average and median values for each *Kp* level are represented by asterisks and squares, respectively. The triangles reflect the 25th and 75th percentiles which are an indicator for the variation of the measurements. The solid line shows the least squares fit of the averaged values, which yields the approximate linear relation between flow speed and *Kp* of $v_{sw} = 365 + 32\ Kp$.

The Weimer electric potential model is based on DE 2 electric field measurements binned by IMF conditions as observed by ISEE 3 or IMP 8. Coverage for the entire high-latitude ionosphere is achieved by spherical harmonic least error fits of the satellite measurements. The model depends on the dipole tilt angle, the solar wind velocity, and the IMF components $B_{\rm y}$ and $B_{\rm z}$. Unlike the Sojka model, the parameters of the Weimer model cannot be reduced to *Kp*. Instead, functional relations between *Kp* and the solar wind parameters were found by least squares fits from a large body of solar wind measurements retrieved from the National Space Science Data Center (NSSDC) OMNIWeb database. Figures 4–6 show the correlations of the solar wind speed, IMF magnitude, and southward angle of the IMF with *Kp*. The functions obtained can only be understood as rough estimates since the spread of the measurements at each *Kp* level is rather large. The linear correlation coefficients of the three dependencies are 0.24, 0.40, and 0.61, respectively. These values are fairly high, considering that the number of observations in the OMNI data set used for this study is nearly 80,000. The probability of a random, uncorrelated data set showing correlation coefficients of this magnitude

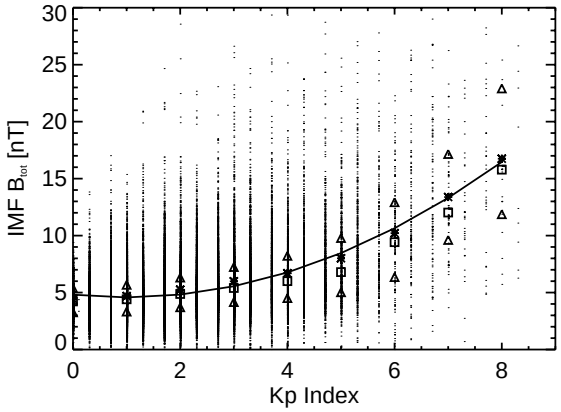

Figure 5. Relationship between the magnitude of the interplanetary magnetic field and *Kp*. The *Kp* dependence is approximated as $B_{\rm tot} = 4.81 - 0.48\,Kp + 0.24\,Kp^2$. The plot symbols are described in the caption of Figure 4.

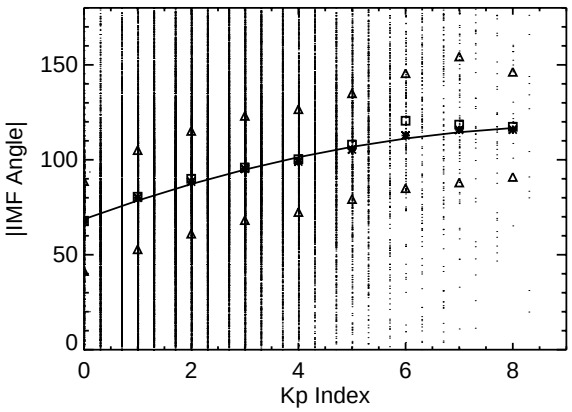

Figure 6. Relationship between the southward angle of the interplanetary magnetic field and *Kp*. The *Kp* dependence is approximated as $\alpha_{\rm IMF} = 68.7 + 10.3\,Kp - 0.5\,Kp^2$. The plot symbols are described in the caption of Figure 4.

is virtually zero. However, the uncertainty of the functional dependence between the solar wind parameters and *Kp* is an additional source of error, and the results obtained with the Weimer model have to be evaluated with care.

3. Model Comparison

The results of the statistical analysis of spin-averaged electron and proton fluxes from paper 1 are reproduced in Plates 1 and 2, respectively. Flux values are displayed color-coded as a function of local time and the *Kp* index, where black regions indicate data unavailability, and white bins contain flux values exceeding the maximum of the corresponding color bar. The energy channels selected correspond to $\sim$ 30, 10, 3, and 1 keV, covering a broad spectrum of plasma sheet energies measured by the Los Alamos Magnetospheric Plasma Analyzer (MPA) instrument (see paper 1). The white lines show the analytically determined geosynchronous Alfvén boundary crossings from the previous work, which correspond to a dipole magnetic field and a *Kp*-dependent Volland-Stern electric potential pattern for a shielding factor of $\gamma = 2$, while the white dots indicate boundary crossings calculated numerically as described above for the same model. By default, the Volland-Stern model does not depend on geomagnetic activity. However, the cross-tail electric field strength in the model may be expressed as a function of the inner edge of the electron plasma sheet at midnight. In the ionosphere this boundary maps to the invariant latitude of the equatorward edge of the diffuse aurora at midnight, which has been determined from Defense Meteorological Satellite Program (DMSP) measurements of precipitating plasma sheet electrons and has been shown to be well correlated with *Kp* [*Gussenhoven et al.*, 1981, 1983]. A detailed description of the *Kp* parameterization of the Volland-Stern model is given in paper 1. The agreement of the numerically obtained boundary crossings with the analytical results from the previous work demonstrates the validity of the numerical algorithm.

The comparisons between the analytical Volland-Stern and dipole model and the more sophisticated model combinations are shown in Figures 7–12. The plot format of Figures 7–12 is identical to that of Plates 1 and 2 except that the color-coded fluxes are omitted. Closed drift trajectory regions are grey-shaded in Figures 7–12. Where no grey-shading is indicated, the Alfvén boundaries separate particle paths passing the Earth on the dawnside from duskside trajectories. Figures 7 and 8 show the boundary crossings calculated with the McIlwain E5D/M2 model for electrons and protons, respectively. The boundaries obtained from the ionospheric electric potential models, all used in combination with a tilted dipole plus Tsyganenko 89c magnetic field,

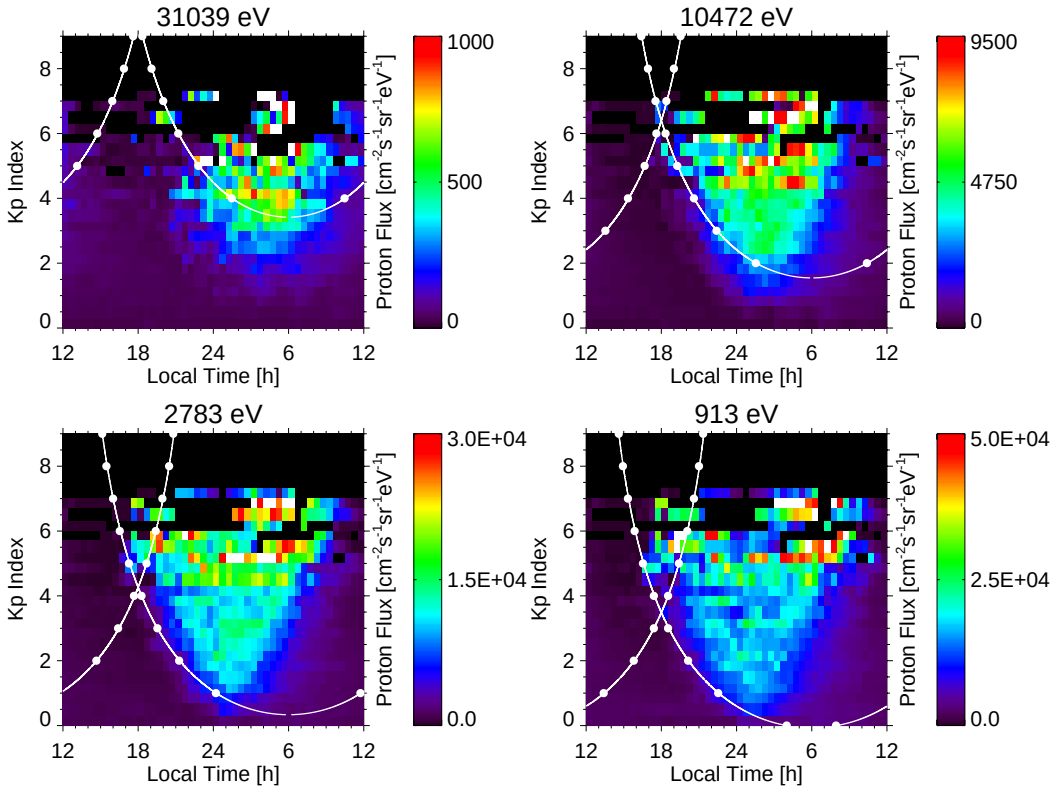

Plate 1. The 1997 averaged electron flux statistics for energy channels near 30, 10, 3, and 1 keV, binned according to LT and *Kp*. Black indicates no data available, and white bins contain fluxes that exceed the corresponding maximum of the color bar. The Alfvén boundary crossings at geosynchronous orbit, indicated by white dots, are numerically evaluated using a dipole magnetic field and a Volland-Stern electric potential with a shielding factor of $\gamma = 2$. The solid curves show analytically calculated boundaries using the same parameters.

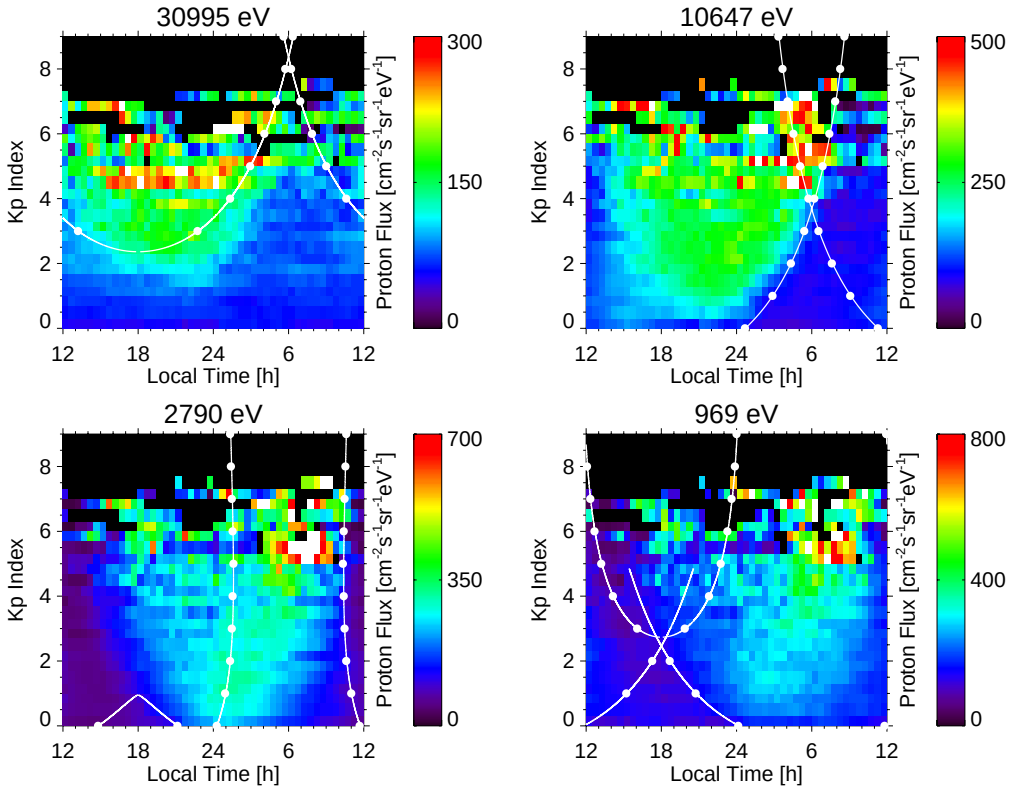

Plate 2. The 1997 averaged proton flux statistics for energy channels near 30, 10, 3, and 1 keV, binned according to LT and *Kp*. Black indicates no data available, and white bins contain fluxes that exceed the corresponding maximum of the color bar. The Alfvén boundary crossings at geosynchronous orbit, indicated by white dots, are numerically evaluated using a dipole magnetic field and a Volland-Stern electric potential with a shielding factor of $\gamma = 2$. The solid curves show analytically calculated boundaries using the same parameters.

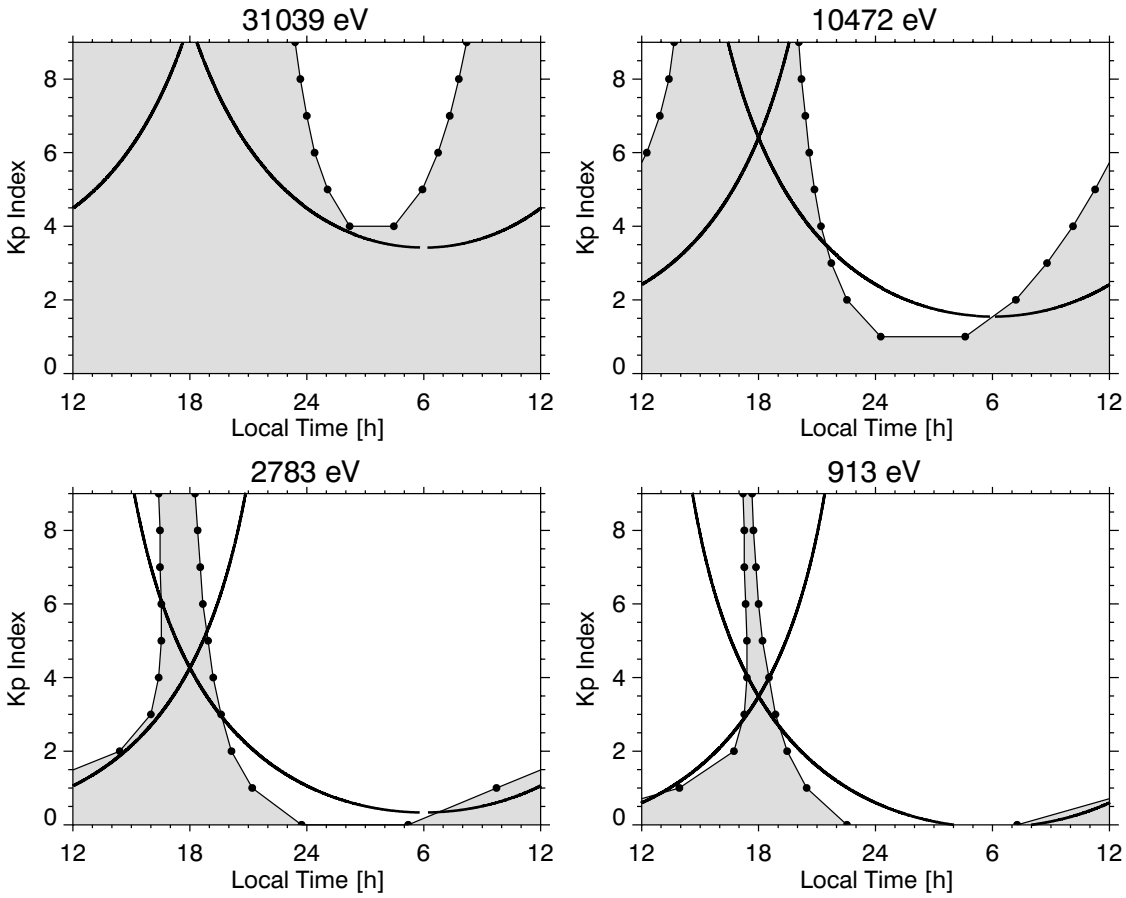

Figure 7. Comparison of electron Alfvén boundary crossings obtained with McIlwain E5D/M2 (dotted line) and Volland-Stern and dipole model (solid line). The plot format is identical to that of Plates 1 and 2 except for the omission of the color-coded fluxes. Regions associated with closed drift trajectories are grey-shaded.

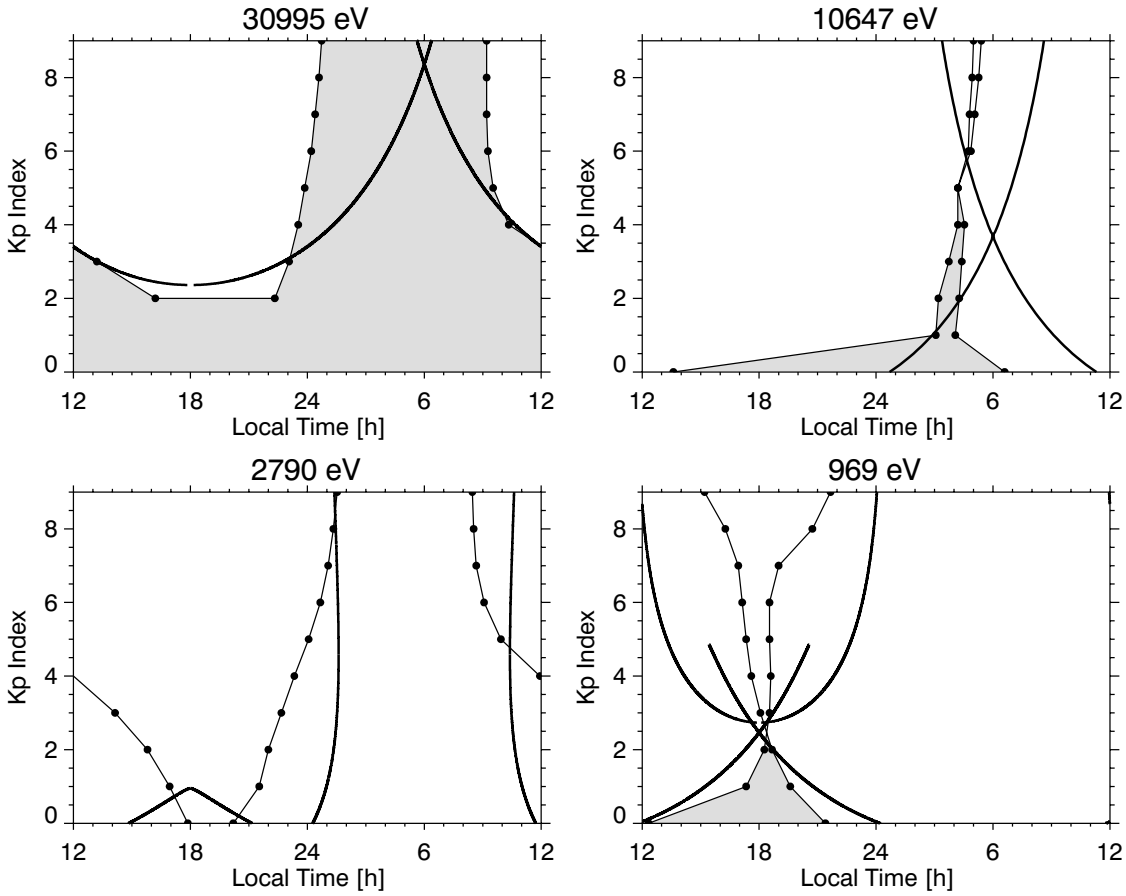

Figure 8. Comparison of proton Alfvén boundary crossings obtained with McIlwain E5D/M2 (dotted line) and Volland-Stern and dipole model (solid line). The plot format is identical to that of Plates 1 and 2 except for the omission of the color-coded fluxes. Regions associated with closed drift trajectories are grey-shaded.

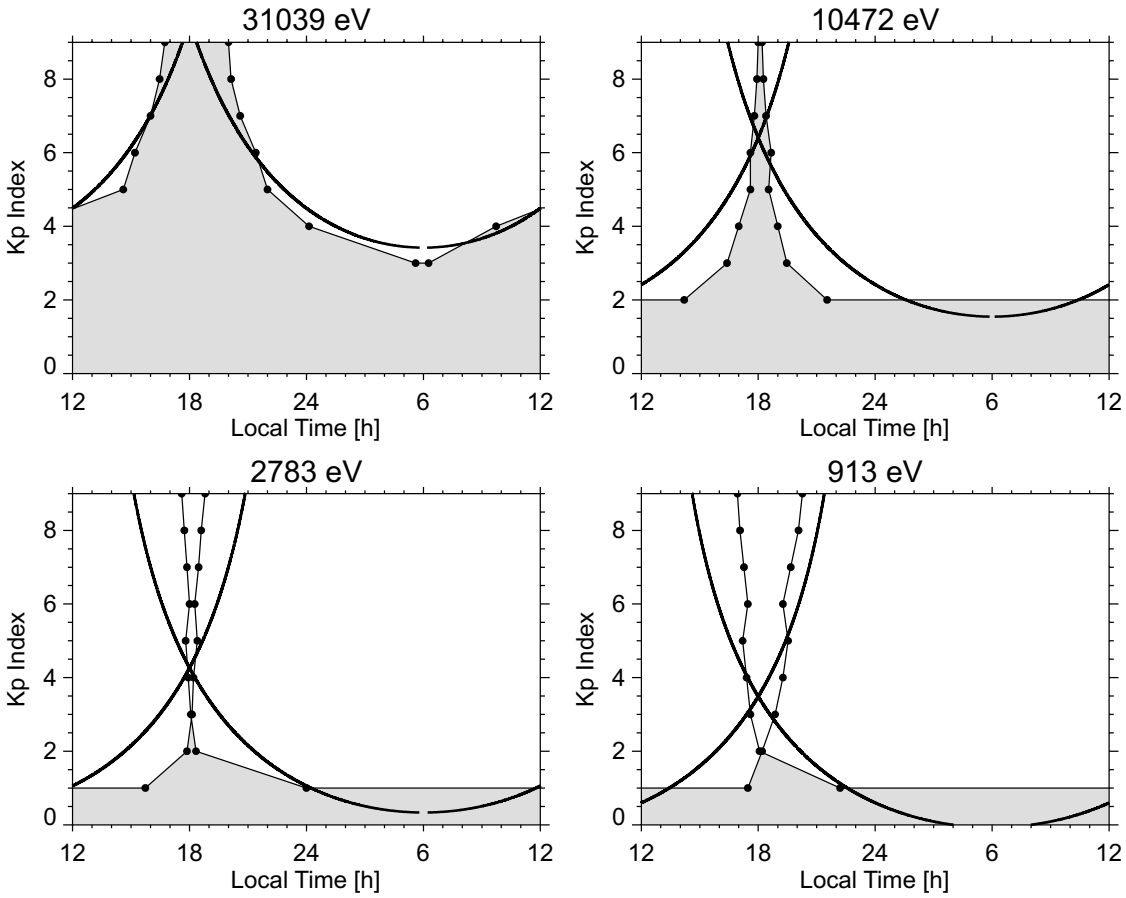

Figure 9. Comparison of electron Alfvén boundary crossings obtained with Sojka 86 and dipole+T89c model (dotted line) and Volland-Stern and dipole model (solid line). The plot format is identical to that of Plates 1 and 2 except for the omission of the color-coded fluxes. Regions associated with closed drift trajectories are grey-shaded.

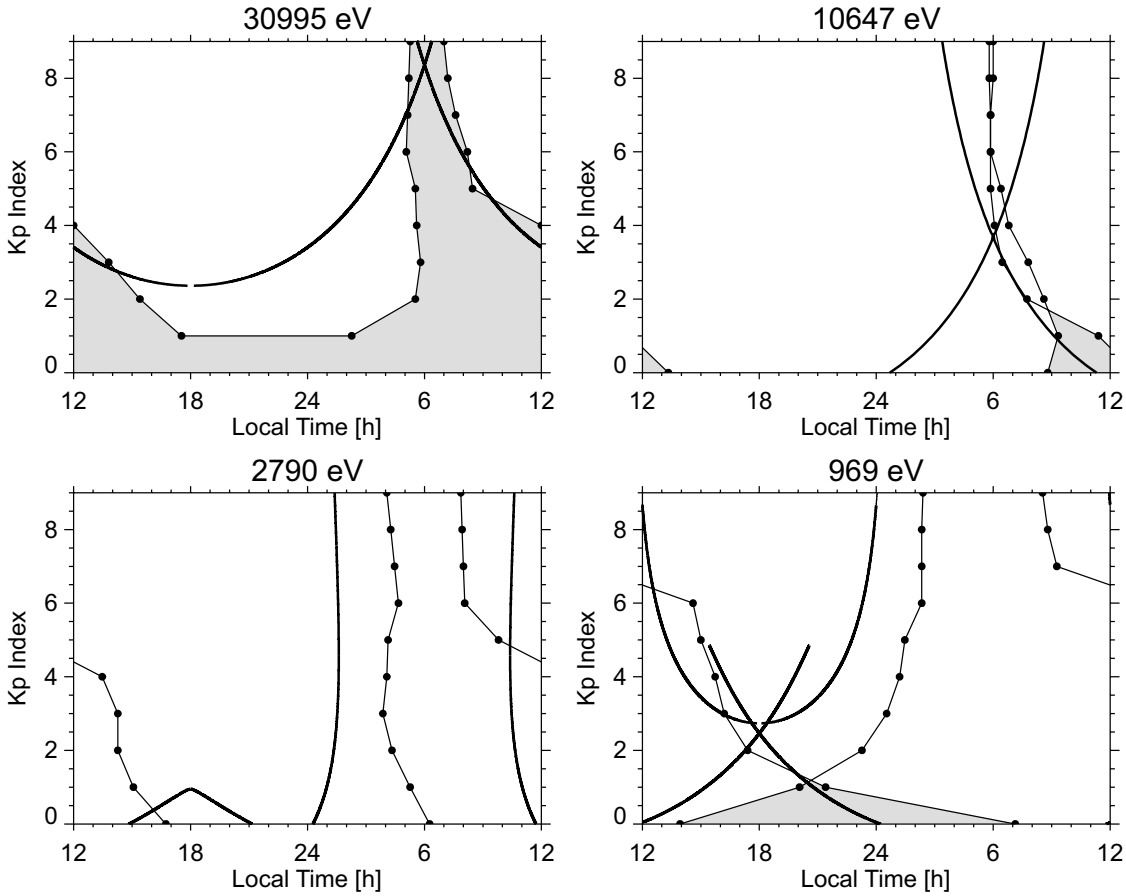

Figure 10. Comparison of proton Alfvén boundary crossings obtained with Sojka 86 and dipole+T89c model (dotted line) and Volland-Stern and dipole model (solid line).

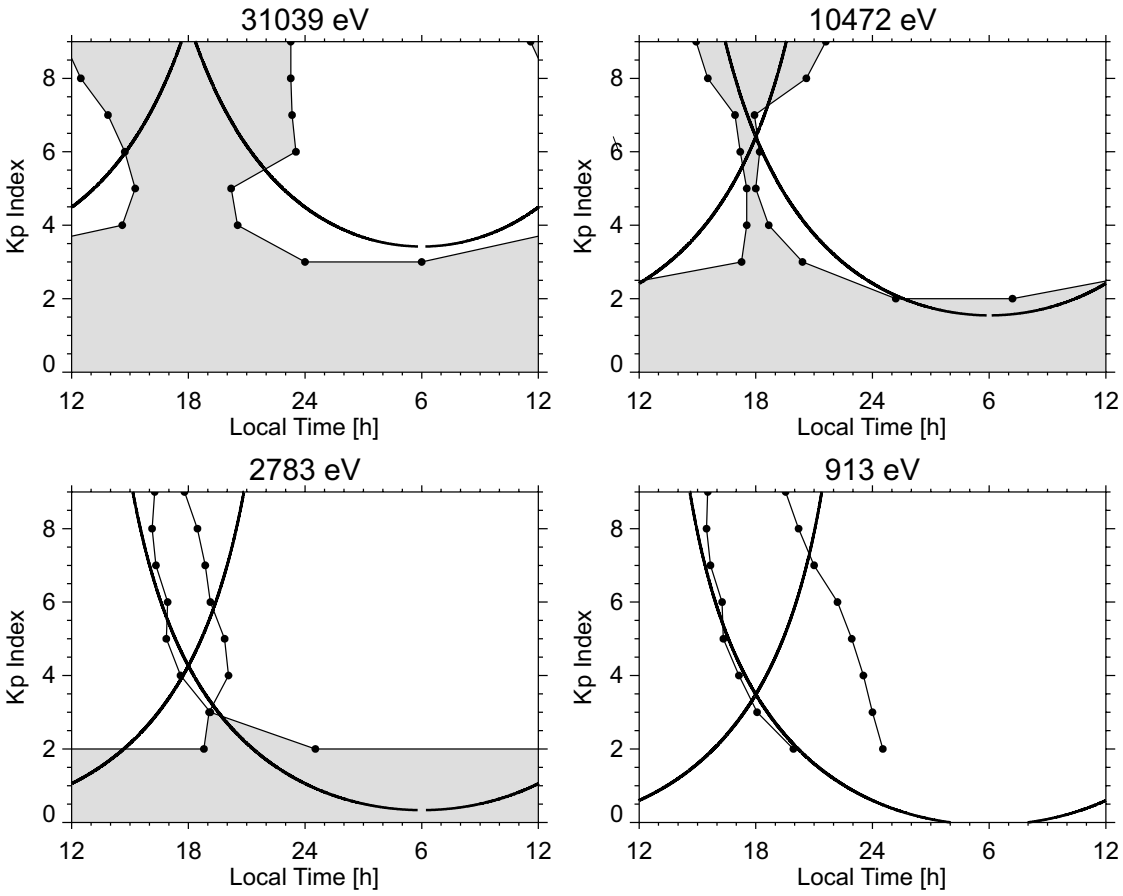

Figure 11. Comparison of electron Alfvén boundary crossings obtained with Heppner-Maynard-Rich and dipole+T89c model (dotted line) and Volland-Stern and dipole model (solid line).

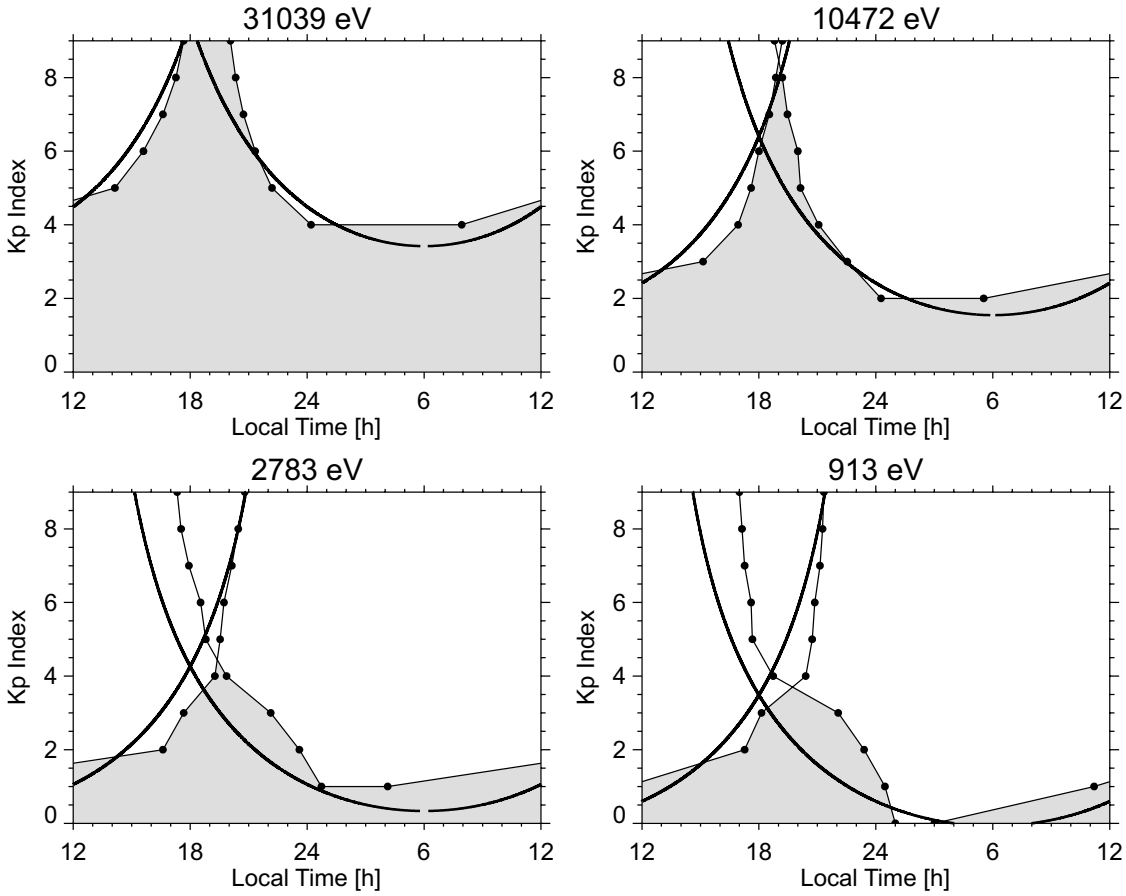

Figure 12. Comparison of electron Alfvén boundary crossings obtained with Weimer 96 and dipole+T89c model (dotted line) and Volland-Stern and dipole model (solid line).

are presented in Figures 9–12. While both electron and proton boundaries are shown for the Sojka 86 electric potential (Figures 9 and 10, respectively), only electron boundaries are illustrated for the Heppner-Maynard-Rich and the Weimer 96 models (Figures 11 and 12, respectively).

For the most part, the Alfvén boundary crossings obtained from the E5D/M2 model for electrons and protons compare well with the observations, in some cases exceeding the quality of the Volland-Stern and dipole model. This is especially true for the energy channels 10 keV and below. Only the 30-keV channels, especially of the electrons, disagree with the observations and show an open trajectory region that is too small compared to the observed fluxes.

The electron Alfvén boundary crossings determined from the Sojka 86 model (Figure 9) are similar to the ones from the Volland-Stern and dipole model. However, comparison with Plate 1 shows that the shape of the numerically evaluated boundary curves does not provide a better interpretation for the observations than do the boundaries obtained from the analytical model. The proton boundaries (Figure 10) support this suggestion and even show that the Volland-Stern and dipole curves describe the observations appreciably better (Plate 2).

Figure 11 shows that like the Sojka model, the Heppner-Maynard-Rich model does not reproduce the observed electron flux boundaries better than the Volland-Stern model. On the other hand, electron flux boundaries determined from the Weimer model (Figure 12) are at least as good as, if not better, than the Volland-Stern boundaries. However, the proton boundaries for these models (not shown) prove to be inferior to the Volland-Stern and dipole proton boundaries.

All graphs shown here are computed for the equinox period. However, the results turn out to be essentially the same for other seasons.

4. Discussion

The observed geosynchronous particle fluxes presented in this and the previous study are statistical averages over a whole year's worth of data. Consequently, comparison with any field model can only be done in a statistical sense that averages over the influence of any dynamic effects. However, the magnetic field and electric potential models used in this work similarly average over the detailed temporal variability of the geomagnetic activity, thus eliminating the dynamic effects as a reason for major discrepancies between the models and the observations.

The Alfvén boundary crossings calculated from the analytical Volland-Stern and dipole model fit the observations remarkably well on the nightside, considering the simplicity of this model. On the dayside the observed boundaries are not solely access-related. Loss processes such as auroral precipitation of the electrons and charge exchange of the protons with exospheric neutrals diminish the fluxes significantly on their drift around the Earth. This is particularly true for lower-energy particles that not only have slower drift speeds but also execute their drifts closer to the Earth than do higher-energy particles. The loss processes are described in more detail in paper 1.

The E5D electric potential model and the M2 magnetic field model were especially designed for use in the inner magnetosphere. Both models are fits to geosynchronous observations made by ATS satellites, which explains the good match of the boundary crossings calculated from this model with the statistical observations of the MPA instrument. However, the convection electric field strength of the E5D model, which is linearly scaled with *Kp*, seems to be underestimated during active periods (see the upper portion of the various panels in Figures 7 and 8). This conclusion is supported by *Maynard and Chen* [1975] where a nonlinear growth of the convection electric field with *Kp* was proposed. Another reason for differences between the model and observational boundaries is the use of the M2 magnetic field model for a wide range of *Kp*. The M2 model was originally derived for geomagnetically quiet periods and may not be valid during active times.

The relatively less satisfactory results obtained from the ionospheric electric potential models used in combination with the Tsyganenko 89c magnetic field model are a surprise that needs to be investigated in more detail. One question to be addressed is whether it is primarily the different convection model or the different magnetic model that most affects the boundary location. The impact of the electric and magnetic field models on the crossing locations can be examined separately by substituting only one numerical model at a time. Choosing the analytical Volland-Stern and dipole model as a base, we compare the well-fit boundary crossings of this model with the Volland-Stern and dipole+T89c and the Sojka and dipole combinations. The electron boundary crossings obtained from the Volland-Stern and dipole+T89c and the Sojka and dipole models are shown in Figures 13 and 14, respectively. The Sojka model is merely an example; other potential models give qualitatively similar results.

The graphs in Figure 13 show that the inclusion of an external magnetic field model in addition to the dipole leads to significant deviations from the base model. Comparison to Plate 1 shows that the resulting boundary curves still compare reasonably well to the observations but with no dramatic improvements relative to the dipole results. The most distinctive difference seen in Figure 13 is an enhanced closed region at dawn in the lower-energy channels. This region is likely to be an artifact of the analysis technique. The

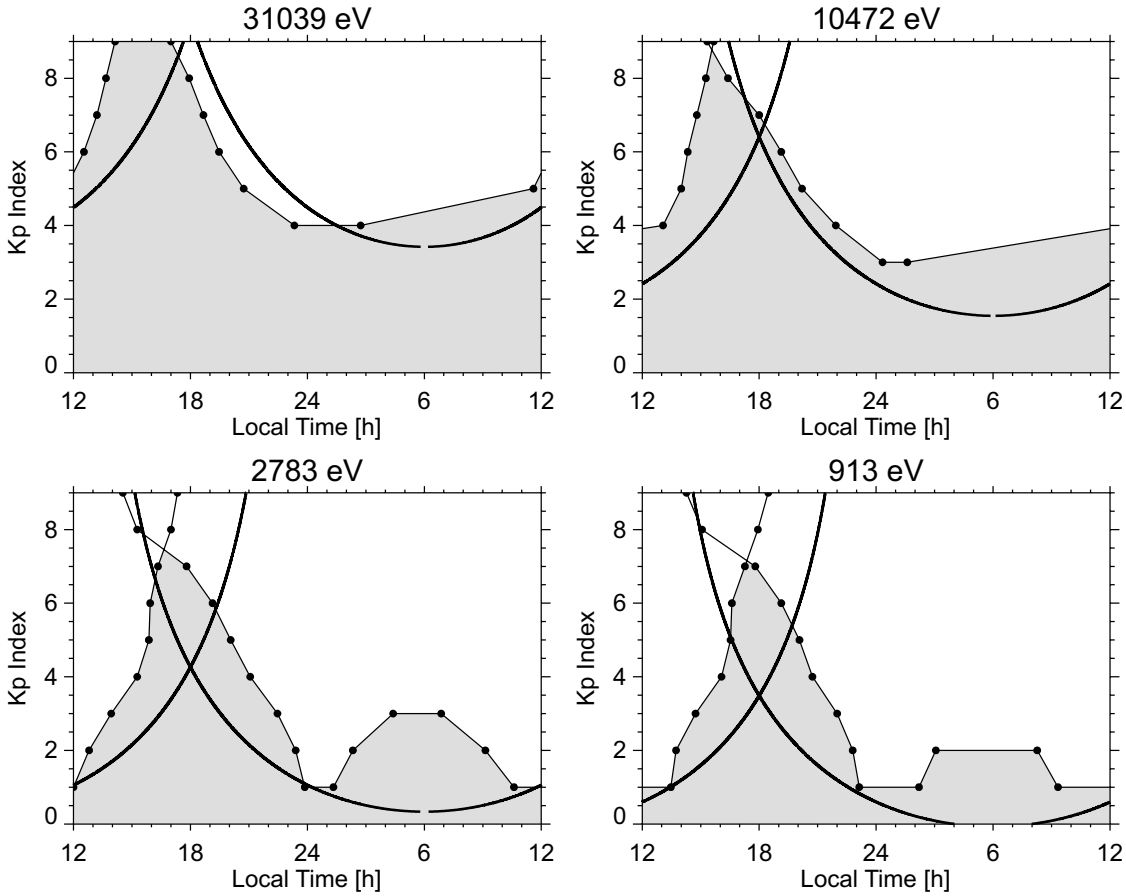

Figure 13. Comparison of electron Alfvén boundary crossings obtained with Volland-Stern and dipole+T89c model (dotted line) and Volland-Stern and dipole model (solid line).

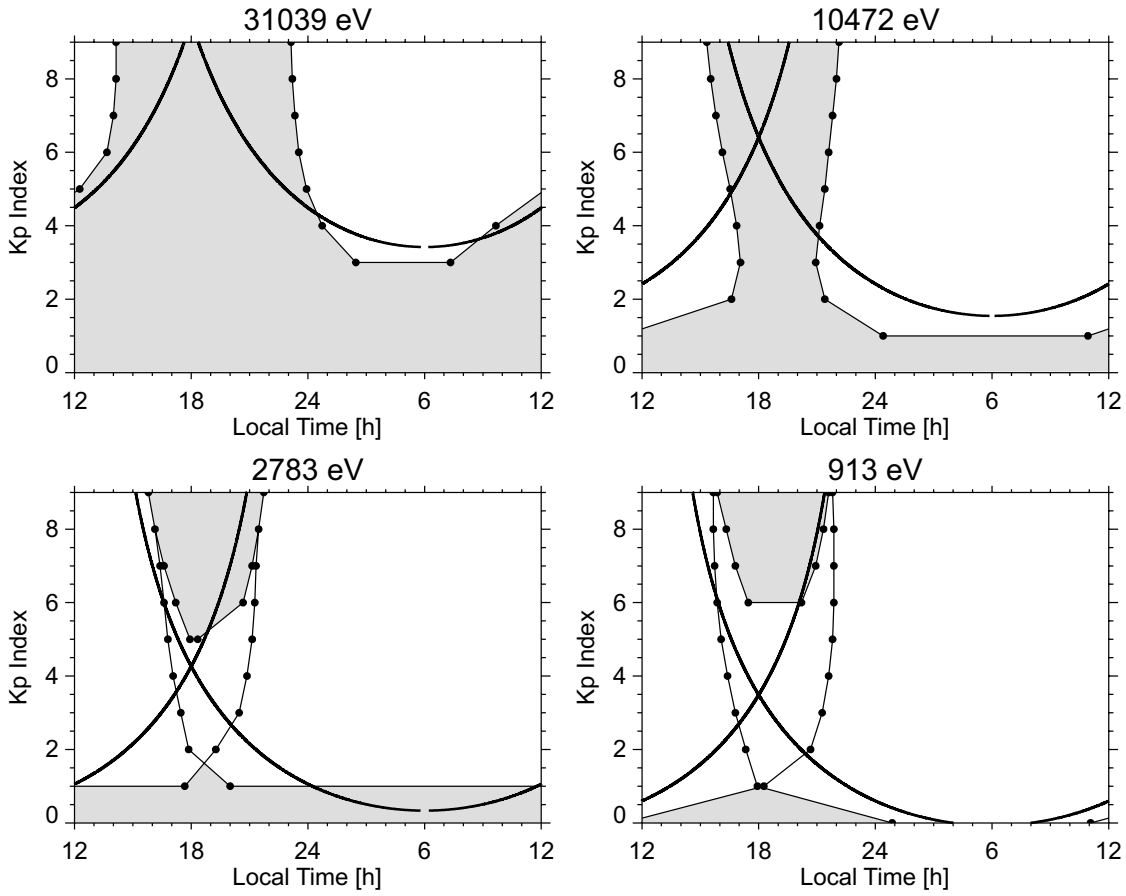

Figure 14. Comparison of electron Alfvén boundary crossings obtained with Sojka and dipole model (dotted line) and Volland-Stern and dipole model (solid line).

open/closed region type is resolved far down the tail at low magnitudes of the magnetic field. At these distances the terminators are located very close to the magnetopause, where the validity of the magnetic field model and the mapping of the ionospheric potential models are questionable. However, the observations do not definitively rule out the existence of such a region. Low fluxes are indeed observed in this region, but we suspect that they are more likely to be caused by flux decay due to auroral electron precipitation as suggested in the previous work rather than a closed orbit region.

The boundary crossings in Figure 14, showing the Sojka and dipole model, provide a significantly worse match to the observed flux boundaries compared to the analytical model. The most obvious difference from the simple model is a larger closed region at high *Kp* for higher energies. Moreover, closed drift orbits that do not encircle the Earth form in the dusk sector during high activity. These drift paths are often referred to as "banana" orbits [cf. *Roederer*, 1970; *Sheldon and Gaffey*, 1993]. These high-*Kp* effects can not be compared to observations, owing to a lack of sufficient statistical coverage of high-activity intervals.

The best correspondence between the observed flux boundaries and the theoretical Alfvén boundaries calculated from the Sojka model is achieved by substitution of both electric and magnetic field models simultaneously, as shown in Figure 9.

Of all models examined, only the lower-energy boundaries of the McIlwain E5D/M2 combination and the electron boundaries obtained from the Weimer and dipole+T89c model reproduce the observed boundaries as well as or better than the Volland-Stern and dipole analytical model. All other models lead to less satisfactory boundary representations. However, since the high-energy boundaries of the McIlwain E5D/M2 model and the proton boundaries of the Weimer and dipole+T89c model are very questionable, we conclude that in spite of its lack of sophistication, the Volland-Stern and dipole model combination still provides the best description of the statistical access of the plasma sheet to geosynchronous orbit. We emphasize again that we may be pushing the high-latitude models beyond their appropriate limits. Thus a disagreement between these models and the geosynchronous observations does not imply the general invalidity of the models but rather emphasizes the need for better convection models in the region examined in this study.

5. Summary

In this paper we expanded on previous work by *Korth et al.* [1999], developing a numerical technique to determine the Alfvén boundary crossings of geosynchronous orbit, using the (U, B, K) technique. Numerical analysis as opposed to analytic expressions has the advantage of allowing the use of arbitrary, empirical electric potential and magnetic field models that may be more accurate than simple analytical models. However, our calculations show that not only is the use of more sophisticated models more complicated and time-consuming, but the models we have examined so far do not provide a better representation of the observed, statistical flux boundaries than does the Volland-Stern and dipole model. This result emphasizes the need for caution in extrapolating high-latitude convection models into the near-Earth region.

An additional problem we encountered in this work is that artificial boundary crossings can at times be produced by numerical difficulties of the Hamiltonian approach. Problems occur especially whenever the open/closed determination is done at low magnitudes of the magnetic field ($\lesssim$ 30 nT). Considering the numerical complications, computation time, and the fact that the sophisticated models do not provide better insight into the average plasma sheet delivery to geosynchronous orbit than does the Volland-Stern and dipole model, we find the analytical model to be more satisfactory for describing the average statistical picture. Nevertheless, since the problems in applying the numerical algorithm to the various convection and magnetic field models were primarily encountered at low B (large distances from the Earth), the (U, B, K) approach described in this study can still be very effectively used to examine drift paths closer to the Earth (e.g., near and inside of geosynchronous orbit), preferably with convection models tailored to near-Earth conditions.

Acknowledgments. The authors would like to express their appreciation to R. B. Sheldon and E. C. Whipple for many helpful discussions on the (U, B, K) coordinate system. This work was carried out under the auspices of the U. S. Department of Energy, with partial support from the NASA SR+T program and the NSF Space Weather program.

Janet G. Luhmann thanks Frederick J. Rich and Margaret W. Chen for their assistance in evaluating this paper.

References

Cummings, W. D., P. J. Coleman, and G. L. Siscoe, Quiet day magnetic field at ATS-1, *J. Geophys. Res.*, *76*, 926–932, 1971.

Gussenhoven, M. S., D. A. Hardy, and W. J. Burke, DMSP/F2 electron observations of equatorward auroral boundaries and their relationship to magnetospheric electric fields, *J. Geophys. Res.*, *86*, 768–778, 1981.

Gussenhoven, M. S., D. A. Hardy, and N. Heinemann, Systematics of the equatorward diffuse auroral boundary, *J. Geophys. Res.*, *88*, 5692–5708, 1983.

Heppner, J. P., and N. C. Maynard, Empirical high-latitude electric field models, *J. Geophys. Res.*, *92*, 4467–4489, 1987.

Hilmer, R. V., and G. P. Ginet, A magnetospheric specification model validation study: Geosynchronous electrons, *J. Atmos. Terr. Phys.*, *62*, 1275–1294, 2000.

Kistler, L. M., and D. J. Larson, Testing electric and magnetic field models of the storm-time inner magnetosphere, *J. Geophys. Res.*, *105*, 25,221–25,231, 2000.

Korth, H., M. F. Thomsen, J. E. Borovsky, and D. J. McComas, Plasma sheet access to geosynchronous orbit, *J. Geophys. Res.*, *104*, 25,047–25,061, 1999.

Maynard, N. C., and A. J. Chen, Isolated cold plasma regions: Observations and their relation to possible production mechanisms, *J. Geophys. Res.*, *80*, 1009–1013, 1975.

McIlwain, C. E., Plasma convection in the vicinity of the geosynchronous orbit, in *Earth's Magnetospheric Processes*, edited by B. M. McCormac, pp. 268–279, D. Reidel, Norwell, Mass., 1972.

McIlwain, C. E., A *Kp* dependent equatorial electric field model, *Adv. Space Res.*, *6(3)*, 187–197, 1986.

Ober, D. M., J. L. Horwitz, and D. L. Gallagher, Formation of density troughs embedded in the outer plasmasphere by subauroral ion drift event, *J. Geophys. Res.*, *102*, 14,595–14,602, 1997.

Pulkkinen, T. I., D. N. Baker, R. J. Pellinen, J. Büchner, H. E. J. Koskinen, R. E. Lopez, R. L. Dyson, and L. A. Frank, Particle scattering and current sheet stability in the geomagnetic tail during the substorm growth phase, *J. Geophys. Res.*, *97*, 19,283–19,297, 1992.

Quinn, J. M., et al., EDI convection measurements at 5–6 R_E in the post-midnight region, *Ann. Geophys.*, *17*, 1503–1512, 1999.

Rich, F. J., and N. C. Maynard, Consequences of using simple analytical functions for the high-latitude convection electric field, *J. Geophys. Res.*, *94*, 3687–3701, 1989.

Roederer, J. G., *Physics and Chemistry in Space*, vol. 2, *Dynamics of Geomagnetically Trapped Radiation*, Springer-Verlag, New York, 1970.

Schield, M. A., J. W. Freeman, and A. J. Dessler, A source for field-aligned currents at auroral latitudes, *J. Geophys. Res.*, *74*, 247–256, 1969.

Sheldon, R. B., and J. D. Gaffey, Particle tracing in the magnetosphere: New algorithms and results, *Geophys. Res. Lett.*, *20*, 767–770, 1993.

Sojka, J. J., C. E. Rasmussen, and R. W. Schunk, An interplanetary magnetic field dependent model of the ionospheric convection electric field, *J. Geophys. Res.*, *91*, 11,281–11,290, 1986.

Stern, D. P., Motion of a proton in the equatorial magnetosphere, *J. Geophys. Res.*, *80*, 595–599, 1975.

Toivanen, P. K., Effects of the large-scale electric field on particle drifts in the near-Earth tail, *J. Geophys. Res.*, *102*, 2405–2415, 1997.

Tsyganenko, N. A., A magnetospheric magnetic field model with a warped tail current sheet, *Planet. Space Sci.*, *37*, 5–20, 1989.

Vogt, J., and K.-H. Glaßmeier, On the location of trapped particle populations in quadrupole magnetospheres, *J. Geophys. Res.*, *105*, 13,063–13,071, 2000.

Volland, H., A semiempirical model of large-scale magnetospheric electric fields, *J. Geophys. Res.*, *78*, 171–180, 1973.

Volland, H., Models of global electric fields within the magnetosphere, *Ann. Geophys.*, *31*, 159–173, 1975.

Volland, H., A model of the magnetopsheric electric convection field, *J. Geophys. Res.*, *83*, 2695–2699, 1978.

Weimer, D. R., Models of high-latitude electric potentials derived with a least error fit of spherical harmonic coefficients, *J. Geophys. Res.*, *100*, 19,595–19,607, 1995.

Weimer, D. R., A flexible, IMF dependent model of high-latitude electric potentials having "space weather" applications, *Geophys. Res. Lett.*, *23*, 2549–2552, 1996.

Whipple, E. C., et al., Identification of magnetospheric particles that travel between spacecraft and their use to help obtain magnetospheric potential distributions, *J. Geophys. Res.*, *103*, 93–102, 1998.

H. Korth and M. F. Thomsen, Space and Atmospheric Science, Los Alamos National Laboratory, NIS–1, MS D466, Los Alamos, NM 87545. (hkorth@lanl.gov)

Received September 26, 2000; revised January 16, 2001; accepted February 5, 2001.